Nanoscale

Salinity gradient power: Influences of temperature and nanopore size

Journal:	*Nanoscale*
Manuscript ID	NR-ART-10-2015-007563.R1
Article Type:	Paper
Date Submitted by the Author:	11-Dec-2015
Complete List of Authors:	Tseng, Shiojenn; Tamkang University, Mathematics Li, Yu-Ming; National Taiwan University Lin, Chih-Yuan; National Taiwan University, Chemical Engineering; Hsu, Jyh-Ping; National Taiwan University, Chemical Engineering

Salinity gradient power: Influences of temperature and nanopore size

Shiojenn Tseng,[1] Yu-Ming Li,[2] Chih-Yuan Lin,[2] Jyh-Ping Hsu[2*]

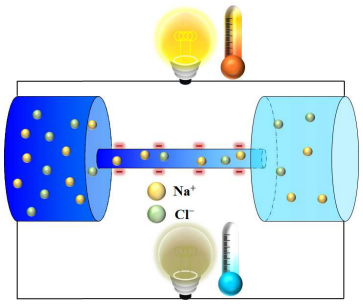

Abstract

Salinity gradient power is a promising, challenging, and readily available renewable energy. Among various methods for harvesting this clean energy, nanofluidic reverse electrodialysis (NRED) is of great potential. Since ionic transport depends highly on the temperature, so is the efficiency of the associated power generated. Here, we conduct a theoretical analysis on the influences of temperature and nanopore size on NRED, focusing on temperature and nanopore size. Results gathered reveal that the maximum power increases with increasing temperature, but the conversion efficiency dependents weakly on temperature. In general, the smaller the nanopore radius or the longer the nanopore the better the ion selectivity is. These results provide desirable and necessary information for improving the performance of NRED as well as designing relevant units in renewable energy plants.

Keywords: salinity gradient power; reverse electrodialysis; temperature effect; size effect

[1]*Department of Mathematics, Tamkang University, New Taipei City, Taiwan 25137*
[2]*Department of Chemical Engineering, National Taiwan University, Taipei, Taiwan 10617*
Tel: 886-2-23637448, Fax: 886-2-23623040, E-mail: jphsu@ntu.edu.tw

1. Introduction

Among the potential resources for renewable energy such as sunlight,[1] wind, tide, waves, and geothermal heat,[2] salinity gradient,[3-9] which generates electrical energy by transferring Gibbs free energy of mixing through nanofluidic reverse electrodialysis (NRED), the main component of which is of nanoscale, is of particular interest. Salinity gradient can be accomplished through connecting two relatively large reservoirs containing different salt concentrations by a nanopore. The salt gradient established drives ions from the high salt concentration reservoir to the low salt concentration reservoir. In particular, if the nanopore is positively (negatively) charged (i.e., ion-selective nanopore), it facilitates transferring of anions (cations) from one reservoir to the other. Adopting an abiotic single-pore nanofluidic energy-harvesting system, Guo *et al.*[10] demonstrated that the Gibbs free energy associated with a salinity gradient can be efficiently converted into electricity. Kim *et al.*[11] showed that in the case of a silica nanopore and an aqueous KCl solution, the highest retrievable power density is 7.7 W/m^2. Cao *et al.*[12] reported that the highest power is ca. 45 pW for the case of a polyimide nanopore and an aqueous KCl solution, and ca. 22 pW for the case of an aqueous NaCl solution. Kim *et al.*[13] found that the highest harvestable power from a NRED with anodic alumina nanopores and aqueous NaCl solution is 542 nW, which is higher than that from other NRED devices. Varying the concentration difference, the pore size of a polycarbonate track-etch (PCTE) membrane, and the types of salt solution, Kwon *et al.*[14] examined the performance of a portable NRED

device. They showed that the electricity generated by monovalent ions is larger than that by bivalent ions. In addition, for the nominal diameter ranging from 15 to 100 nm, the performance of a NRED cell can be enhanced by reducing its pore size. Gao *et al.*[15] proposed using an ionic diode membrane to harvest electric energy from a salinity gradient. They claimed that the power density can be up to 3.46 W/m^2, exceeding appreciably several commercial ion-exchange membranes.

In addition to experimental efforts, several theoretical attempts have also been made in modeling salinity gradient. For instance, Yeh *et al.*[16] examined the influence of the direction of salt gradient on the efficiency of a NRED device with a cone-shaped nanopore. They showed that a nanopore with its base end having a higher salt concentration has a larger energy conversion efficiency than that for the case where its tip end has a higher salt concentration. This observation was attributed to the overlapping of the electrical double layer (EDL) near the tip end of a nanopore. Jeong *et al.*[17] studied numerically the ionic transport in the cell pair of a NRED device. Kang *et al.*[18] studied theoretically the effect of nanopore size on its performance in a NRED device. It was found that the smaller the nanopore radius and/or the higher the salt concentration on the high salt concentration side of the nanopore the larger the power per unit nanopore cross section area. Several other interesting results were also observed, but the rationale behind them was not discussed in detail. For instance, the curves of (power/nanopore cross section area) against nanopore

length for various levels of the salt concentration on the low salt concentration side of the nanopore intersect with each other. In addition, the ratio of (power/nanopore cross section area) can have a local maximum as the nanopore length varies.

Among various factors that might affect the performance of a NRED device, temperature and nanopore size are particularly significant. The influence of the latter is obvious, and that of the former is because almost all the physicochemical properties, such as ionic mobility, permittivity, and viscosity, are temperature dependent. Taghipoor *et al.*,[19] for example, concluded that the electrical conductance of a nanochannel can be influenced significantly by temperature. The translocation of biomolecules through a nanopore is also affected by temperature.[20,21] In fact, several temperature-responsive nanostructural devices have been designed to regulate ionic transport.[22-25] Although various factors have been examined for their influence on the performance of a NRED device, the influence of temperature is seldom discussed. Considering the great potential of harvesting energy by NRED, a detailed understanding of its performance under various conditions is highly desirable and necessary. In this study, attempts are made to assess the performance of a NRED device, focusing on the influences of temperature and nanopore size.

2. Theory

As illustrated in Fig. 1, we consider a cylindrical nanopore of length L_n and radius R_n connecting two same, large cylindrical reservoirs of radius R_r and length L_r. The wall of the

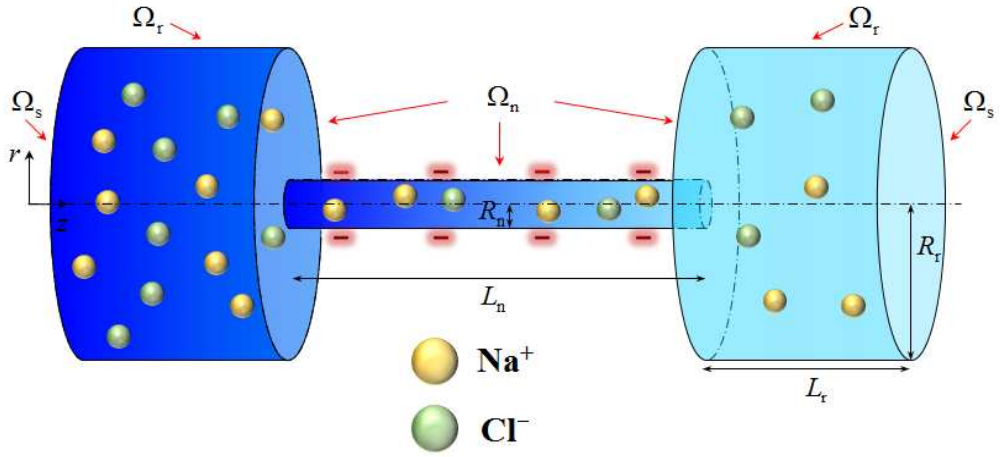

Fig. 1. Transport of ionic species through a cylindrical nanopore of length L_n and radius R_n connecting two same, large cylindrical reservoirs of radius R_r and length L_r. Ω_n, Ω_r and Ω_s are the nanopore wall, the reservoir wall, and the reservoir surface, respectively.

nanopore is charged and that of the reservoirs is free of charge. The bulk salt concentration in the left (right) reservoir is C_H (C_L) with $C_H > C_L$. The cylindrical coordinates are adopted with the origin at the center of the left surface of the left reservoir.

2.1 Governing equations

The present problem can be described by the set of equations below:

$$\nabla^2\phi = -\frac{1}{\varepsilon_r\varepsilon_0}\sum_{i=1}^{N} z_i F C_i \tag{1}$$

$$\mathbf{J}_i = C_i\mathbf{u} - D_i\left(\nabla C_i + \frac{z_i F C_i}{RT}\nabla\phi\right) \tag{2}$$

$$\nabla\cdot\mathbf{J}_i = 0 \tag{3}$$

$$\nabla\cdot\mathbf{u} = 0 \tag{4}$$

$$\mu\nabla^2\mathbf{u} - \nabla p - \rho_f\nabla\phi = 0 \tag{5}$$

ϕ, e, ε_r, ε_0, $\mathbf{u}$, F, R, T, μ, p, ρ_f, and N are the electric potential, the elementary charge, the

relative permittivity, the permittivity of a vacuum, the fluid velocity, Faraday constant, gas constant, the absolute temperature, the fluid viscosity, the pressure, the space charge density, and the number of ionic species, respectively. z_i, C_i, $\mathbf{J}_i$, and D_i are the valence, the concentration, the flux, and the diffusivity of the ith ionic species. Note that ε_r, D_i, and μ are all temperature dependent. For illustration, we consider an aqueous NaCl solution (i.e., N=2) and, for simplicity, we assume its physical properties are essentially the same as those of water. Therefore, the temperature dependence of ε_r is[26,27]

$$\varepsilon_r = \exp[4.47615 - 4.60128\times10^{-3}(\delta T) + 2.6952\times10^{-7}(\delta T)^2] \quad (6)$$

where $\delta T = T - 273.15$, $0 \leqq \delta T \leqq 100$.

The temperature dependence of μ is[28]

$$\mu = 2.414\times10^{-5}\times10^{247.8/(T-140)}, \quad 273.15 \le T \le 643.15 \quad (7)$$

The Nernst-Haskell equation[29,30] is adopted for the temperature dependence of D_i:

$$D_i = \frac{RT}{F^2}\left[\frac{1/|z_i|}{1/\lambda_i^0}\right] \quad (8)$$

λ_i^0 is the limiting conductance of the ith ionic species.

The temperature dependence of λ_i^0 is[31]

$$\lambda_i^0 = \lambda_i^0(298.15) + a(\bar{\delta}T) + b(\bar{\delta}T)^2 + c(\bar{\delta}T)^3, \quad (9)$$

where $\lambda_i^0(298.15)$ is the limiting conductance of the ith ionic species at 298.15 K, $\bar{\delta}T = T - 298.15$, $-20 \leqq \bar{\delta}T \leqq 30$. The values of a, b, and c for Na^+ and Cl^- are listed in Table 1.[31]

Table 1. Values of the parameters used in eqn (9)

	λ_i^0(298.15 K)	a	$b\times10^2$	$c\times10^4$
Na^+	50.15	1.09160	0.47150	-0.1150
Cl^-	76.35	1.54037	0.46500	-0.1285

2.2 Boundary conditions

The system under consideration is symmetric about the nanopore axis, and no pressure gradient is applied across the reservoirs. In addition, we assume the following: (i) The nanopore wall is maintained at a constant charge density $\sigma=\sigma_n$, and the reservoir wall is free of charge ($\sigma=0$). (ii) The wall of nanopore Ω_n and that of reservoir Ω_r are impermeable to ions. (iii) Ω_n is non-slip and Ω_r is slip. Therefore, the following boundary conditions apply:

$$-\varepsilon_r\varepsilon_0\frac{\partial\phi}{\partial n}=\sigma_n \quad \text{on} \quad \Omega_n \tag{10}$$

$$-\varepsilon_r\varepsilon_0\frac{\partial\phi}{\partial n}=0 \quad \text{on} \quad \Omega_r \tag{11}$$

$$\mathbf{n}\cdot\mathbf{J}_i=0 \text{ on } \Omega_n \text{ and } \Omega_r \tag{12}$$

n is the unit outer normal vector, and $\partial/\partial n$ denotes the variation along **n**. In addition, we assume that $\phi=0$ and Ω_s is free of viscous stress.

The electric current I can be evaluated by

$$I=\iint_A\sum_{i=1}^{N}z_i e(\mathbf{n}\cdot\mathbf{J}_i)dA, \tag{13}$$

where A denotes either end of the reservoirs. The selectivity of the nanopore is measured by the transference number t_+

$$t_+=\frac{I_+}{I_+ +|I_-|} \tag{14}$$

I_+ and I_- are the electric currents contributed by cations and anions, respectively, t_+ ranges from 0 to 1. If $0.5< t_+<1$, the nanopore is cation selective; otherwise, it is anion selective. If $t_+=0.5$, the nanopore is not ion selective. In our case, if $0.5< t_+<1$, a nanopore facilitates the transport of Na^+ from the left reservoir (high salt concentration) to the right reservoir (low salt concentration), so that Na^+ (Cl^-) accumulates in the right (left) reservoir. This induces a diffusion potential E_{diff}[32]

$$E_{\text{diff}} = (2t_+ - 1)\frac{RT}{zF}\ln\left(\frac{\gamma_{\text{H}} C_{\text{H}}}{\gamma_{\text{L}} C_{\text{L}}}\right) \tag{15}$$

γ_{H} and γ_{L} are the activity coefficients of the bulk concentrations in left and right reservoirs, respectively. According to Bromley,[33]

$$\log\left(\gamma_{\text{H(L)}}^{1/z_+z_-}\right) = \frac{-0.511 I_s^{1/2}}{1 + I_s^{1/2}} + \frac{\left(0.06 + 0.03444/\rho_{\text{w}}\right) I_s}{\left(1 + \frac{1.5}{|z_+z_-|} I_s\right)^2} + \frac{0.0574 I_s}{|z_+z_-|\rho_{\text{w}}} \tag{16}$$

z_+, z_-, I_s, and ρ_{w} are the valences of cations and anions, the ionic strength, and the density of water,[34] respectively. Note that E_{diff} retards the transfer of Na^+ from the left reservoir to the right reservoir.

If we let Ω be the internal resistance of the nanopore, the electric potential difference of the system under consideration, ΔV, is

$$\Delta V = E_{\text{diff}} - I\Omega, \tag{17}$$

The harvestable electric power is the product of the ionic current and the potential, and since the maximum electric power P_{max} occurs when the electric potential is half the

diffusion potential,

$$P_{\max} = \frac{IE_{\text{diff}}}{2} \tag{18}$$

The corresponding energy conversion efficiency η is defined as the ratio of the retrievable electric power to the Gibbs free energy of mixing[35]

$$\eta = \frac{I\Delta V}{\left(J_+ + J_-\right)RT \ln\left(\frac{\gamma_{\text{H}} C_{\text{H}}}{\gamma_{\text{L}} C_{\text{L}}}\right)} \tag{19}$$

J_+ and J_- are the fluxes of cations and anions, respectively. The efficiency corresponding to the maximum power generation, $\eta_{\max}$, is

$$\eta_{\max} = \frac{\left(2t_+ - 1\right)^2}{2} \tag{20}$$

Note that $\eta_{\max}$ depends on t_+ only.

The present problem is solved by COMSOL (version 4.3a, www.comsol.com) operating in a high performance cluster. Its applicability has been verified previously.[36,37] Typically, the number of meshes elements used is ca. 90000. The behavior of the system under consideration is examined by numerical simulation through varying the nanopore length L_{n}, its radius R_{n}, and the absolute temperature T. For illustration, we assume L_{r}=500 nm, R_{r}=500 nm, and σ_{n}=-0.5 e/nm^2.[10,38,39] In addition, C_{L} is fixed at 1 mM, and C_{H} varies from 10 to 1000 mM.

3. Results and Discussion

Fig. 2 summarizes the dependence of the electric current I on the concentration

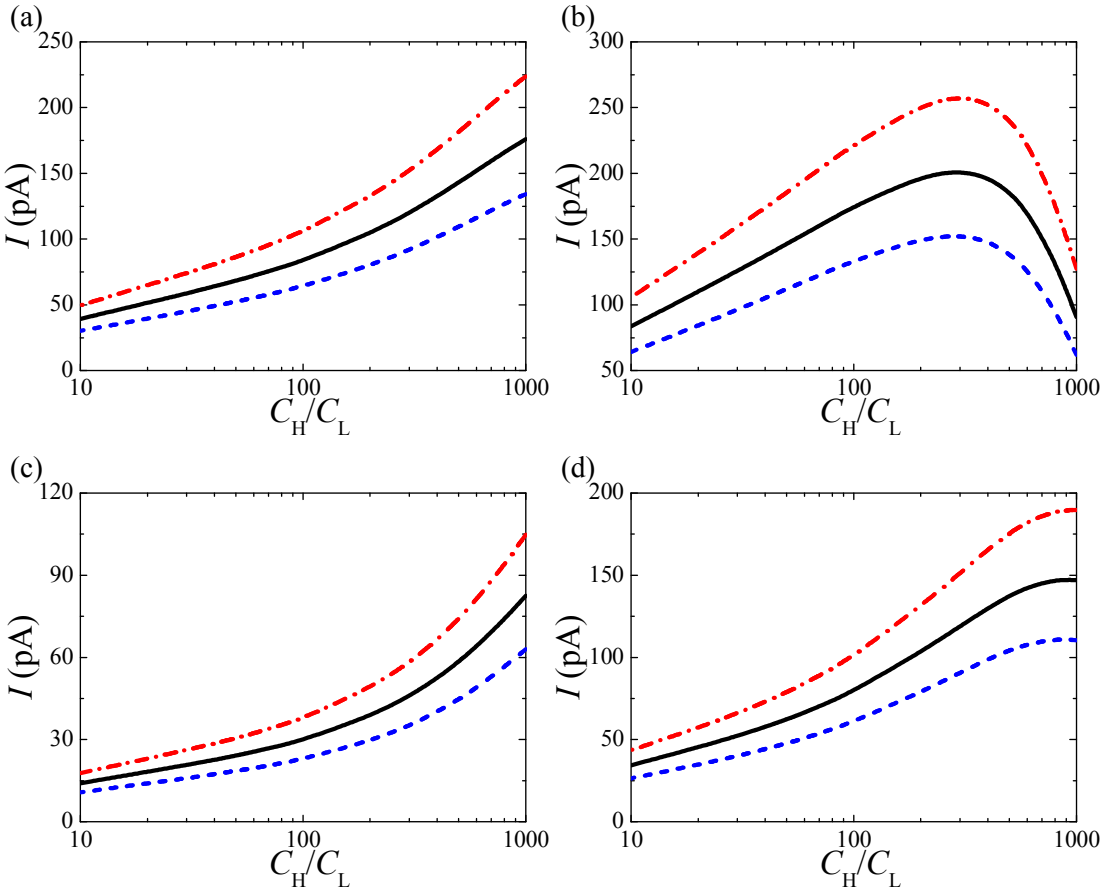

Fig. 2. Variation of the electrical current I with the concentration ratio (C_H/C_L) for various combinations of R_n and L_n at three values of temperature (red curve: 308.15 K; black: 298.15 K; blue: 288.15 K) for R_n=8 nm and L_n=300 nm, (a), R_n=20 nm and L_n=300 nm, (b), R_n=8 nm and L_n=1000 nm, (c), and R_n=20 nm and L_n=1000 nm, (d).

ratio (C_H/C_L) for various combinations of R_n and L_n at three representative levels of temperature.

Fig. 2(a) reveals that the electric current I increases monotonically with increasing temperature. As can be seen in Fig. 3, this results from the increase in the ionic diffusivities with temperature.

Fig. 2(a) shows that at R_n=8 nm and L_n=300 nm, I increases monotonically with

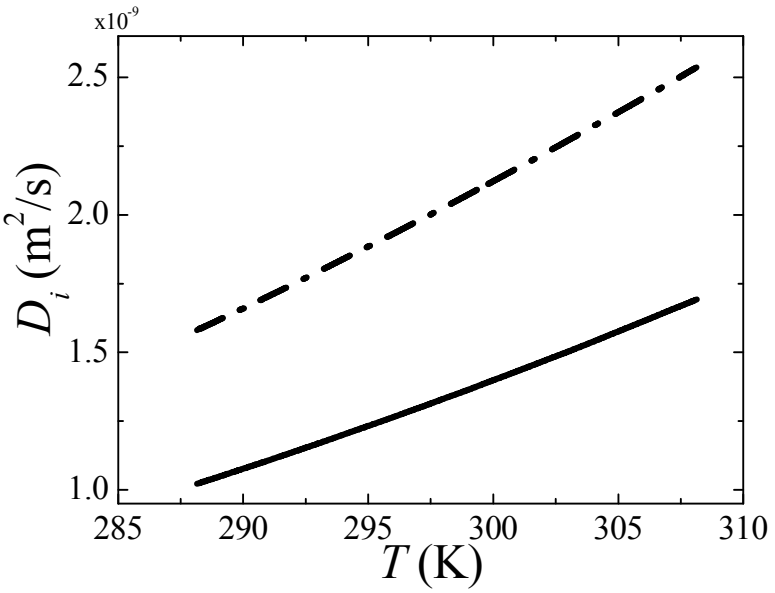

Fig. 3. Temperature dependence of the ionic diffusivity for Na^+ (solid curve) and Cl^- (dotted curve).

increasing (C_H/C_L). However, it is interesting to see in Fig. 2(b) that at R_n=20 nm and L_n=300 nm, I has a local maximum as (C_H/C_L) varies. This is because as (C_H/C_L) increases, although the amount of counterions (Na^+) available for ionic transport through the nanopore increases, the electric double layer[40-41] is thinner at the same time. If the nanopore radius gets larger, EDL overlapping becomes less significant, thereby facilitating the transport of coions (Cl^-), so that the net electric current decreases. This is exemplified in Fig. 4 that for each level of (C_H/C_L), the concentration of Cl^- at R_n=20 nm is higher than that at R_n=8 nm, and the concentration of Cl^- approaches that of Na^+ as (C_H/C_L) increases, yielding the local maximum in Fig. 2(b). If L_n is raised to 1000 nm, it becomes difficult for both counterions and coions to diffuse through the nanopore, especially for the later. Consequently, the concentration of Cl^- near the right-hand side of the nanopore at L_n=1000

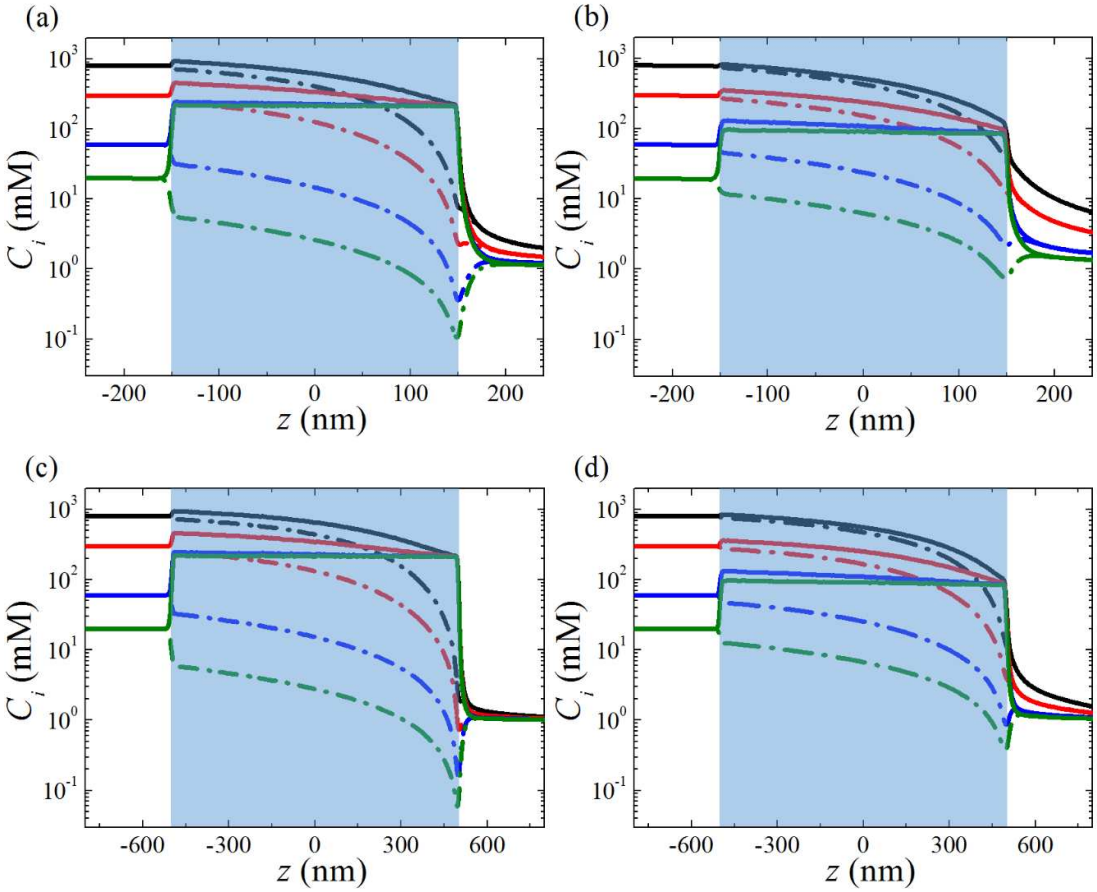

Fig. 4. Axial variation in the cross sectional averaged ionic concentration for T=298.15 K at R_n=8 nm and L_n=300 nm, (a), R_n=20 nm and L_n=300 nm, (b), R_n=8 nm and L_n=1000 nm, (c), R_n=20 nm and L_n=1000 nm, (d). Solid (dotted) curve: Na^+ (Cl^-). Black curve: C_H/C_L=800; red: C_H/C_L=300; blue: C_H/C_L=60, green curve: C_H/C_L=20. The shaded region highlights the nanopore interior.

nm is lower than that at L_n=300 nm. In addition, because the rate of decrease in the concentration of Cl^- is much faster than that of Na^+, I does not show a local maximum in Fig. 2(d).

Fig. 5 summarizes the variations of the transference number t_+ and the conversion efficiency η_{max} with (C_H/C_L). This figure suggests that the influence of the temperature on t_+ is inappreciable, so is that on η_{max}. This is because for a fixed value of (C_H/C_L), t_+ is essentially a function of the ionic diffusivities, and is proportional to $D_+/(D_++D_-)$, which

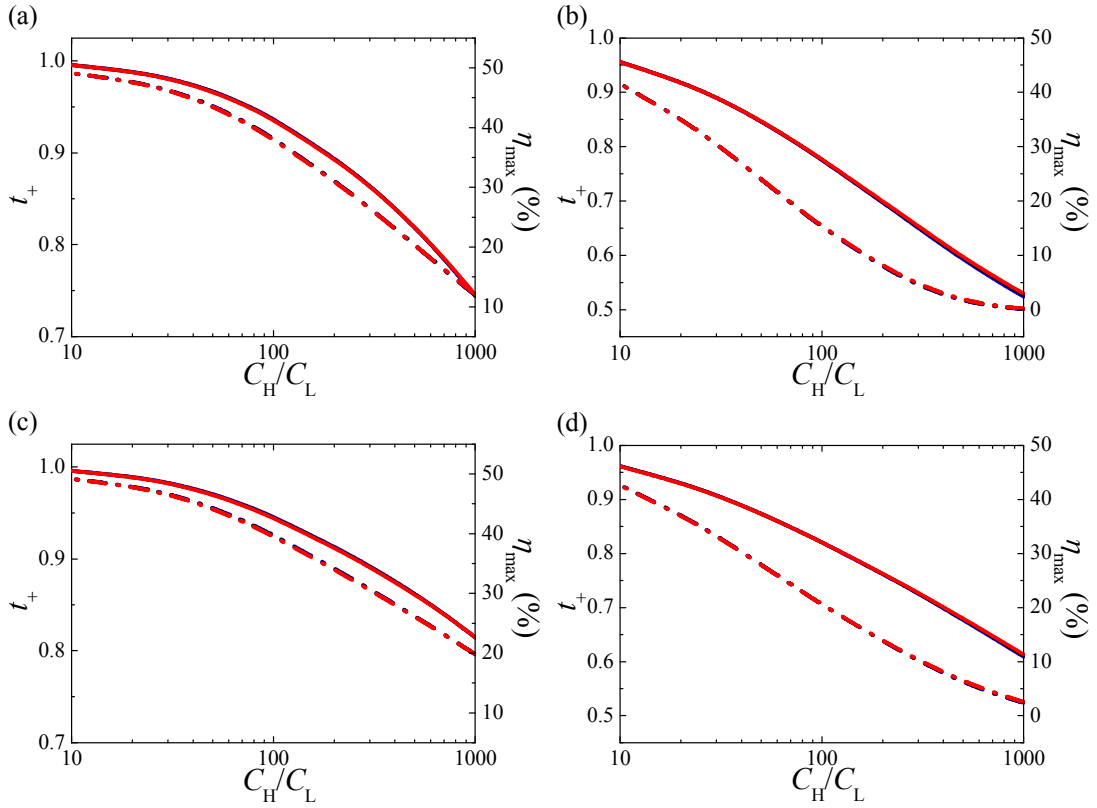

Fig. 5. Variation of the transference number t_+ and the maximum conversion efficiency η_{max} with the concentration ratio (C_H/C_L) for various combinations of R_n and L_n at three values of temperature (red curve: 308.15 K; black: 298.15 K; blue: 288.15 K) for R_n=8 nm and L_n=300 nm, (a), R_n=20 nm and L_n=300 nm, (b), R_n=8 nm and L_n=1000 nm, (c), and R_n=20 nm and L_n=1000 nm, (d). Solid (dotted) curve: variation of t_+ (η_{max}).

varies only slightly for temperature ranging from 288.15 to 308.15K. Fig. 5 also shows that both t_+ and η_{max} decrease with increasing (C_H/C_L). This arises from the decrease in the electric double layer thickness with increasing (C_H/C_L), as mentioned previously. Therefore, t_+ decreases accordingly, and the nanopore becomes less ion selective. Note that the longer the nanopore (larger L_n) and/or the narrower the nanopore (smaller R_n) the better its selectivity is. This phenomenon is similar to the influence of nanopore size on the electric current. As discussed earlier, the larger the nanopore radius and/or the shorter the nanopore

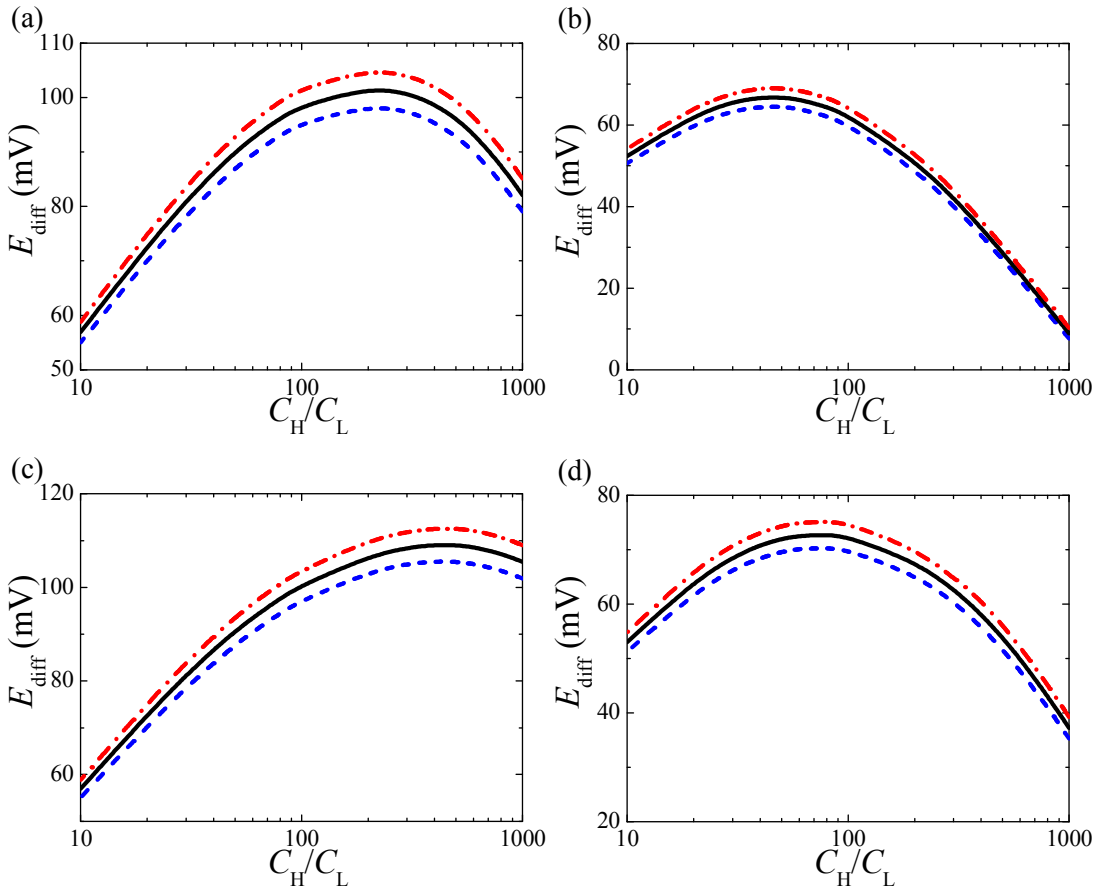

Fig. 6. Variation of the diffusion potential E_{diff} with the concentration ratio (C_H/C_L) for various combinations of R_n and L_n at three values of temperature (red curve: 308.15 K; black: 298.15 K; blue: 288.15 K) for R_n=8 nm and L_n=300 nm, (a), R_n=20 nm and L_n=300 nm, (b), R_n=8 nm and L_n=1000 nm, (c), and R_n=20 nm and L_n=1000 nm, (d).

the easier the transfer of Cl^-, yielding a smaller selectivity. Therefore, the largest selectivity occurs at R_n=8 nm and L_n=1000 nm (Fig. 5(c)) and smallest selectivity at R_n=20 nm and L_n=300 nm (Fig. 5(b)).

According to eqn (15), E_{diff} varies with t_+, T, and $\ln(\gamma_H C_H/\gamma_L C_L)$. Since compared with that of $\ln(C_H/C_L)$, the change of $\ln(\gamma_H/\gamma_L)$ is unimportant, we consider the influence of $\ln(C_H/C_L)$ only. As can be seen in Fig. 6, the higher the temperature the larger the E_{diff}, which is expected from eqn (15). All the curves in Fig. 6 show a local maximum as

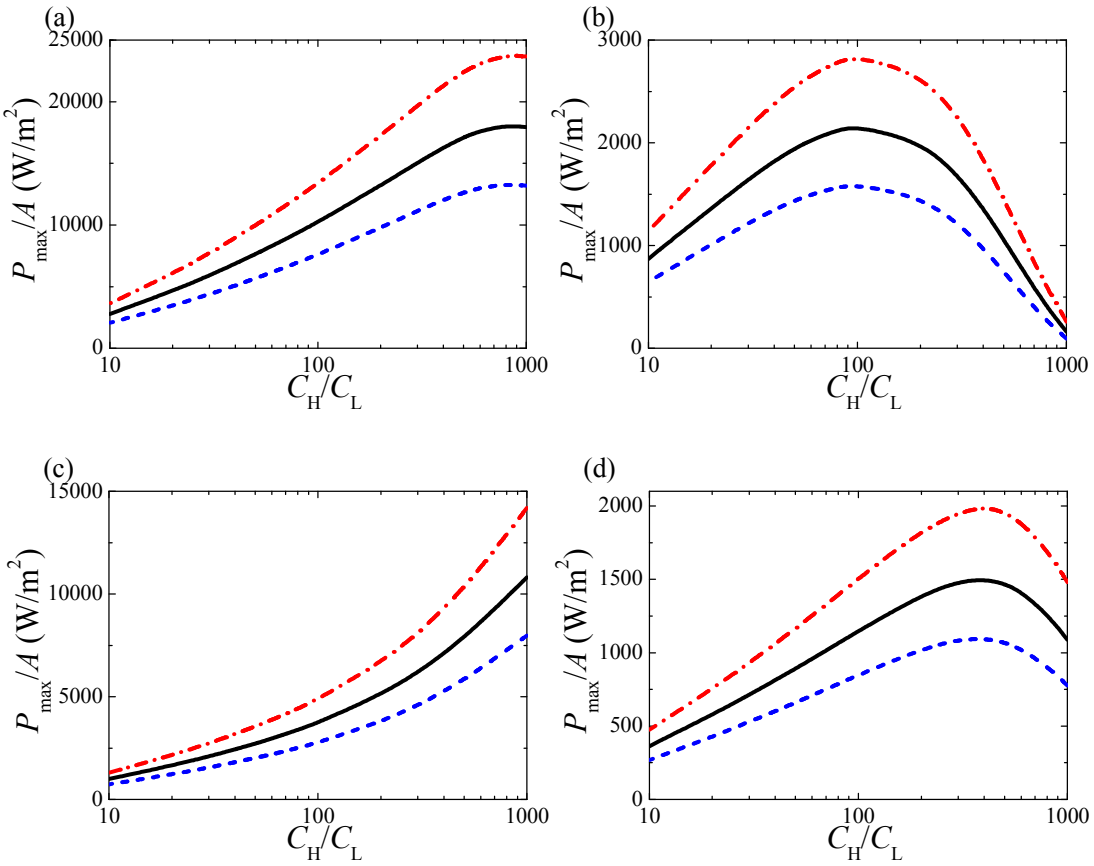

Fig. 7. Variation of the maximum power per unit cross-sectional nanopore area (P_{max}/A) with the concentration ratio (C_H/C_L) for various combinations of R_n and L_n at three values of temperature (red curve: 308.15 K; black: 298.15 K; blue: 288.15 K) for R_n=8 nm and L_n=300 nm, (a), R_n=20 nm and L_n=300 nm, (b), R_n=8 nm and L_n=1000 nm, (c), and R_n=20 nm and L_n=1000 nm, (d).

$\ln(C_H/C_L)$ varies. This is because although E_{diff} increases with increasing $\ln(C_H/C_L)$, t_+ decreases at the same time, as seen in Fig. 5, leading to a smaller E_{diff}. The former (latter) dominates at small (large) $\ln(C_H/C_L)$, yielding a local maximum in E_{diff}. As mentioned previously, E_{diff} comes from the asymmetric distributions in Na^+ and Cl^-, retarding the transfer of Na^+. If t_+ is large, implying that the amount of Na^+ transfer is large and, therefore, a higher E_{diff} is needed to retard its transfer. The maximal value of E_{diff} occurs at R_n=8 nm and L_n=1000 nm (Fig. 6(c)), and the minimal value at R_n=20 nm and L_n=300 nm

(Fig. 6(b)), which are consistent with the trends of t_+ seen in Fig. 5.

Fig. 7 illustrates the variation of the maximum power per unit cross-sectional nanopore area (P_{max}/A) with the concentration ratio (C_H/C_L) for various combinations of R_n and L_n at three values of temperature. Since both the electric current I and the diffusion potential E_{diff} increase with increasing temperature, the higher the temperature the larger the (P_{max}/A). A comparison between the results for R_n=8 nm and those for R_n=20 nm reveals that the (P_{max}/A) in the latter has a local maximum as (C_H/C_L) varies. In addition, the (P_{max}/A) at R_n=20 nm is smaller than that at R_n=8 nm. This behavior is similar to that of E_{diff} in Fig. 6. A comparison between the results for L_n=300 nm and those for L_n=1000 nm indicates that the (P_{max}/A) in the former is larger than that in the latter. This behavior is similar to that of I in Fig. 2. Therefore, the largest (P_{max}/A) occurs at R_n=8 nm and L_n=300 nm (Fig. 6(a)), and smallest (P_{max}/A) at R_n=20 nm and L_n=1000 nm (Fig. 6(d)).

Conclusions

We modeled theoretically the salinity gradient power based on nanopore/nanochannel reverse elecrtodialysis (NRED), focusing on the influences of temperature and nanopore size. The results of numerical simulation reveal that these factors are significant in designing a NRED device. For instance, because a larger electric current I and a higher diffusion potential E_{diff} can be achieved at an elevated temperature, a higher maximum power per unit nanopore cross-sectional area (P_{max}/A) can be harvested. However, the

transference number of cations t_+ and the maximum conversion efficiency η_{max} are influenced only slightly due to that the ionic diffusivities of cations and anions increase with temperature at similar rate. We show that the smaller the nanopore radius R_n and/or the longer the nanopore length L_n the better the ion selectivity and, therefore the larger the η_{max}. This arises from the influence of electric double layer (EDL): the degree of EDL overlapping is serious if R_n is small, and it is difficult for ions, especially coions, to diffuse through the nanopore. It is interesting to observe that the electric current I has a local maximum as the concentration ratio (C_H/C_L)=(bulk salt concentration in the high salt concentration reservoir/bulk salt concentration in the low salt concentration reservoir) varies at R_n=20 nm and L_n=300 nm, which is attributed to that the transport of coions in this case is easier than that in other cases. Due the competition between (C_H/C_L) and t_+, E_{diff} shows a local maximum for each combination of R_n and L_n. For (C_H/C_L) ranges from 10 to 1000 and T from 288.15 to 308.15 K, since E_{diff} is influenced mainly by t_+, it has the largest value at R_n=8 nm and L_n=1000 nm, occurring at (C_H/C_L) $\cong$ 400 and $T \cong$ 308.15 K. In general, more power can be harvested at about the same conversion efficiency with higher temperature. Because $I(L_n=300\ nm)>I(L_n=1000\ nm)$, and $E_{diff}(R_n=8\ nm)>E_{diff}(R_n=20\ nm)$, ($P_{max}/A$) has the largest value at L_n=300 nm and R_n=8nm.

References

1. B. Oregan, M. Gratzel, *Nature*, 1991, **353**, 737-740.

2. O. Ellabban, H. Abu-Rub, F. Blaabjerg, *Renewable Sustainable Energy Rev.*, 2014, **39**, 748-764.

3. R. E. Pattle, *Nature*, 1954, **174**, 660.

4. A. J. Bard, L. R. Faulkner, *Electrochemical Methods: Fundamentals and Applications*. John Wiley & Sons, New York, 2001.

5. J. W. Post, J. Veerman, H. V. M. Hamelers, G. J. W. Euverink, S. J. Metz, K. Nymeijer, C. J. N. Buisman, *J. Membr. Sci.*, 2007, **288**, 218-230.

6. B. E. Logan, M. Elimelech, *Nature*, 2012, **488**, 313-319.

7. W. Guo, Y. Tian, L. Jiang, *Acc. Chem. Res.*, 2013, **46**, 2834-2846.

8. A. Siria, P. Poncharal, A. L. Biance, R. Fulcrand, X. Blase, S. T. Purcell, L. Bocquet, *Nature*, 2013, **494**, 455-458.

9. N. Y. Yip, D. A. Vermaas, K. Nijmeijer, M. Elimelech, *Environ. Sci. Technol.*, 2014, **48**, 4925-4936.

10. W. Guo, L. X. Cao, J. C. Xia, F. Q. Nie, W. Ma, J. M. Xue, Y. L. Song, D. B. Zhu, Y. G. Wang, L. Jiang, *Adv. Funct. Mater.*, 2010, **20**, 1339-1344.

11. D. K. Kim, C. H. Duan, Y. F. Chen, A. Majumdar, *Microfluid. Nanofluid.*, 2010, **9**, 1215-1224.

12. L. X. Cao, W. Guo, W. Ma, L. Wang, F. Xia, S. T. Wang, Y. G. Wang, L. Jiang, D. B. Zhu, *Energy Environ. Sci.*, 2011, **4**, 2259-2266.

13. J. Kim, S. J. Kim, D. K. Kim, *Energy*, 2013, **51**, 413-421.

14. K. Kwon, S. J. Lee, L. N. Li, C. Han, D. Kim, *Int. J. Energy Res.*, 2014, **38**, 530-537.

15. J. Gao, W. Guo, D. Feng, H. T. Wang, D. Y. Zhao, L. Jiang, *J. Am. Chem. Soc.*, 2014, **136**, 12265-12272.

16. H. C. Yeh, C. C. Chang, R. J. Yang, *RSC Adv.*, 2014, **4**, 2705-2714.

17. H. I. Jeong, H. J. Kim, D. K. Kim, *Energy*, 2014, **68**, 229-237.

18. B. D. Kang, H. J. Kim, M. G. Lee, D. K. Kim, *Energy*, 2015, **86**, 525-538.

19. M. Taghipoor, A. Bertsch, P. Renaud, *ACS Nano*, 2015, **9**, 4563-4571.

20. D. Fologea, J. Uplinger, B. Thomas, D. S. McNabb, J. L. Li, *Nano Lett.*, 2005, **5**, 1734-1737.

21. L. H. Yeh, M. K. Zhang, S. W. Joo, S. Z. Qian, *Electrophoresis*, 2012, **33**, 3458-3465.

22. B. Yameen, M. Ali, R. Neumann, W. Ensinger, W. Knoll, O. Azzaroni, *Small*, 2009, **5**, 1287-1291.

23. W. Guo, H. W. Xia, F. Xia, X. Hou, L. X. Cao, L. Wang, J. M. Xue, G. Z. Zhang, Y. L. Song, D. B. Zhu, Y. G. Wang, L. Jiang, *ChemPhysChem*, 2010, **11**, 859-864.

24. X. Hou, F. Yang, L. Li, Y. L. Song, L. Jiang, D. B. Zhu, *J. Am. Chem. Soc.*, 2010, **132**, 11736-11742.

25. S. Nasir, M. Ali, W. Ensinger, *Nanotechnology*, 2012, **23**, 225502-225511.

26. B. B. Owen, C. E. Milner, R. C. Miller, H. L. Cogan, *J. Phys. Chem.*, 1961, **65**,

2065-2070.

27. S. J. Tseng, J. Y. Lin, J. P. Hsu, *Anal. Chim. Acta*, 2014, **847**, 80-89.

28. T. Al-Shemmeri, *Engineering Fluid Mechanics*, Ventus Publishing ApS, 2012.

29. J. P. Hsu, Y. H. Tai, L. H. Yeh, S. J. Tseng, *Langmuir*, 2012, **28**, 1013-1019.

30. W. M. Haynes, D. R. Lide, T. J. Bruno, *CRC Handbook of Chemistry and Physics*, CRC Press, Boca Raton, 2015.

31. H. S. Harned, B. B. Owen, *The Physical Chemistry of Electrolytic Solutions*, Reinhold, New York, 1958.

32. J. Cervera, A. Alcaraz, B. Schiedt, R. Neumann, P. Ramirez, *J. Phys. Chem. C*, 2007, **111**, 12265-12273.

33. L. A.Bromley, *AIChE J.*, 1973, **19**, 313-320.

34. M. Tanaka, G. Girard, R. Davis, A. Peuto, N. Bignell, *Metrologia*, 2001, **38**, 301-309.

35. J. C. Fair, J. F. Osterle, *J. Chem. Phys.*, 1971, **54**, 3307-3316.

36. L. H. Yeh, C. Hughes, Z. P. Zeng, S. Z. Qian, *Anal. Chem.*, 2014, **86**, 2681-2686.

37. L. H. Yeh, M. K. Zhang, S. Z. Qian, *Anal. Chem.*, 2013, **85**, 7527-7534.

38. C. Y. Lin, L. H. Yeh, J. P. Hsu, S. Tseng, *Small*, 2015, **11**, 4594-4602.

39. I. Vlassiouk, S. Smirnov, Z. Siwy, *Nano Lett.*, 2008, **8**, 1978-1985.

40. L. Joly, C. Ybert, E. Trizac, L. Bocquet, *Phys. Rev. Lett.*, 2004, **93**, 257805.

41. C. Largeot, C. Portet, J. Chmiola, P. L. Taberna, Y. Gogotsi, P. Simon, *J. Am. Chem.*

Soc., 2008, **130**, 2730-2731.